CrystEngComm

Accepted Manuscript

ROYAL SOCIETY OF CHEMISTRY

www.rsc.org/crystengcomm

Synthesis of g-C_3N_4-sensitized and $NaNbO_3$-substrated II-type heterojunction with enhanced photocatalytic degradation activity

Song Chengjie[a,b], Fan Mingshan[b], Hu Bo[b], Chen Tianjun[b], Wang Liping*[,a], Shi Weidong*[,b]

[a] School of Environmental and Safety Engineering, Changzhou University, Changzhou, 213164, P. R. China;

[b] School of Chemistry and Chemical Engineering, Jiangsu University, Zhenjiang, 212013, P. R. China.

E-mail: wlp@cczu.edu.cn; shiwd999@163.com

Abstract

The g-C_3N_4 (CN) sensitized and $NaNbO_3$ (NN) substrated II-type heterojunction (g-C_3N_4/$NaNbO_3$) is prepared by solid phase calcination method with urea and NN. The layered CN is anchoring on the surface of cubic NN. The samples are characterized by XPS, UV–vis spectroscopy, FE-SEM, XRD and FT-IR. The photodegradation mechanism of RhB solutions under visible light irradiation is investigated. Electron paramagnetic resonance (ESR) and radical scavenger experiments reveal that the main active specie is $O_2^{\bullet-}$ and the OH• also plays a role in the photodegradation process. Compared with pure CN, the CN/NN hybrid materials display much excellent photocatalytic activity for rhodamine b (RhB), methyl orange (MO) and tetracycline (TC) degradation under visible-light irradiation. The 8-CN/NN sample shows highest degradation rate (1.888h^{-1}) and it is 2.7 times than that of pure CN (0.697). The photodegradation of RhB, MO and TC all fit to pseudo first order kinetics by all CN/NN photocatalysts. The photocatalysts also possess great stability. The exploration of CN/NN photocatalyst is significant for the further practical application of photocatalysis in wastewater treatment.

1. Introduction

In recent years, environmental pollution and energy shortages have become the focus of world attention. Since the pathbreaking work of Fujishima and Honda[1], photocatalysis has become a promising technology for degradation of environmental pollutants and production of hydrogen[2-7]. A series of metal based photocatalysts such as transition-metal oxides[8, 9], metal nitrides[10, 11], metal sulphides[12] and so on have been developed and researched pollutants degradation and solar energy conversion.

However, the metal photocatalysts are expensive and limited, as primary catalysts. Recently, the nonmetal compound—graphitic carbon nitride (g-C_3N_4, simply as CN) has attracted more and more research interest, due to it is stable, environmental, economic and efficient[13-16]. CN owns great surface properties that are important to photocatalysis, such as basic surface functionalities, electron-rich properties, H-bonding motifs, etc. and photocatalytic properties[17, 18]. And its suitable bandgap (~2.7 eV) can be driven by visible light, which improves solar energy utilization efficiency greatly, with high oxidation power of valance band (VB) holes[19, 20]. It also exhibits high thermal and chemical stability and nontoxicity, owing to its tri-s-triazine ring structure and high degree of condensation[21, 22]. However, its photocatalytic activity remains limited by the rapid recombination rate of photoinduced electrons and holes[23, 24]. Efforts to improve the photocatalytic activity of CN include loading cocatalysts on the surface of CN[25], doping[26], designing appropriate textural properties[27] and preparing composites or heterojunctions with other semiconductors[28, 29]. In all these efforts, heterostructure is the most frequently used method. The heterostructure can improve the separation between photoinduced holes and electrons, especially, the type-II heterostructure can prolong exciton lifetime by increasing the spatial separation of the electron and hole[30].

Recently, $NaNbO_3$ (simply as NN) has attracted much attention because of its excellent physical and chemical property properties[31-33]. The NN, with a typical perovskite structure, owns a range of useful properties, such as good chemical stability, low environmental impact, low cost, abundance and high crystallinity. NN is a promising photocatalyst for photocatalytic application, and there are few articles about photocatalytic degradation of pollutants. The photocatalysts, such as $NaNbO_3$/ZnO[34], In_2O_3/$NaNbO_3$[35] and $NaNbO_3$/Nb_2O_5[36] *et al.* $NaNbO_3$-based composites, have been used in photocatalytic field and have shown excellent photocatalytic activity. NN is an ideal candidate to promote the photocatalytic activity of CN. Shi *et al.* [20] have been synthesized $NaNbO_3$/g-C_3N_4 (simply as NN/CN), and the photocatalysts were applied to fuel production with Pt cocatalyst. Li *et al.* [37] also have been synthesized NN/CN composites successfully, and the photocatalysts were applied to gaseous pollutants degradation. The photocatalytic degradation of RhB were carried out under full arc Xe lamp irradiation, which including UV light and visible light. However, the NN only can be activated by UV light and the CN can be activated by UV and visible light. Under the UV light irradiation, the NN/CN heterojunction is a typical heterostructure model. But the NN/CN heterojunction is a type-II heterostructure model under the visible light irradiation. Unfortunately, the degradation mechanism of RhB in the NN/CN suspension liquid under full arc Xe lamp irradiation is complex and is difficulty to be explored. On the other hand, visible light is more ideal than UV light as light source. Herein, we explore the photocatalytic mechanism of NN/CN under visible light irradiation in pollutants solution with ESR spectrum and active species trapping experiments, and we also find relatively optimized weight ratio between precursor-urea and NN.

In this article, NN is synthesized by the hydrothermal process and x-NN/CN (x=4, 6, 8, 10, 12) photocatalysts are prepared by solid phase calcination method. The

photocatalysts are characterized by XRD, FE-SEM, FT-IR, XPS, UV-Vis DRS and ESR. The results showed that the photocatalytic activities of composites are generally higher than that of pure NN and CN. The prepared samples can degrade RhB, MO and tetracycline (TC) efficiently. The optimized rate constant of RhB degradation is 2.7 times that of pure NN, which is achieved by 8-NN/CN. A possible mechanism for enhancing photocatalytic activity of NN/CN is also proposed in view of the interface interaction of photoinduced carrying transfer and separation. This work plays a significant role in guiding the design of type-II heterojunction with high photocatalytic oxidation and reduction performance.

2. Experimental Section

2.1 Preparation of g-C_3N_4/$NaNbO_3$ hybrid materials

The pure NN photocatalyst is prepared by one step hydrothermal method in the following procedure：2mmol Nb_2O_5 powder is put into 10 mL NaOH solution (8 mol/L) and stirred for 10 min. Then the mixture solution is transferred into a 15 mL of Teflon-lined stainless steel autoclave and keep heating at 200℃ for 24 h. After reaction, the autoclave is cooled to room temperature naturally. The resulting products is washed several times with distilled water and absolute ethanol. Finally, the power is dried at 70℃ for 12h.

For the compounds of CN/NN, 0.05g NN power and several weights (4g, 6g, 8g, 10g and 12g) of urea are dispersed in absolute ethanol and stirred 30 min for homogeneous dispersion. Then the solution is dried at 80℃ for 3h to get dried powder. The powder is calcined at muffle furnace with programmed temperature, with the rate of 2.3℃/min, heating to 550℃ and keeping for 4 hours, the cooled to room temperature naturally. The products of calcining are washed with salpeter solution (0.1mol/L) firstly, then washed with distilled water to neutral pH. The neutral solution is dried, collecting the powder. The composites are marked as 4-CN/NN, 6-CN/NN, 8-CN/NN, 10-CN/NN and 12-CN/NN for the various adding urea weights (4g, 6g, 8g, 10g and 12g).

2.2 Characterization

The products are analyzed by X-ray diffraction (XRD) measurements carried out on X-ray diffraction (Bruker D8 Advance diffractometer) with Cu-Kα radiation in the 2θ range of 5 – 80° at a scanning rate of 7°min^{-1}. The accelerating voltage and the applied current are 50 kV and 300 mA, respectively. The morphologies of the as-prepared samples are observed by the scanning electron microscopy (SEM). SEM observations are conducted by an S-4800 field emission SEM (FESEM, Hitachi, Japan). X-ray photoelectron spectroscopy (XPS) measurements are conducted using a PHI Quantum 2000 XPS system with a monochromatic Al Kα source and a charge neutralizer. The FT-IR spectroscopy are obtained from Fourier Transform Infrared Spectrometer (Thermo Nicolet Corporation, Nicolet Nexus 470). The UV−vis spectra of the products are obtained from a UV–vis spectrophotometer (UV2450, Shimadzu, Japan). BaSO4 is used as a reflectance standard. The radicals are detected by Electron Paramagnetic Resonance Spectrometer (BRUKER, A300-10/12).

2.3 Photocatalytic degradation of dye

Rhodamine B (RhB), methyl orange (MO) and tetracycline (TC) are used as model organic pollutants to evaluate the photocatalytic activity of samples under visible light illumination. The photodegradation of dye solution is carried out at 308 K in a photochemical reactor under visible light(＞420nm). The photo-chemical reactor contained 10mg sample and 100 mL of 10 mg/L RhB solution. To exclude the influence of physical adsorption, the reactor is kept in the dark for 60 min to reach the adsorption equilibrium. A 150 W xenon lamp which is located about 8 cm to one side of the containing solution is used as the light source, which has a glass filter to remove the UV light. At each time interval, photocatalysts are separated by centrifugation at 10000 rpm for 5 min, and the light absorption of clear solution for the different samples is measured by an UV−vis spectrophotometer.

3. Results and Discussion

3.1 Characterization of photocatalysts

The particle size and morphology of NN are shown in Fig.1. The pure NN synthesized with hydrothermal method is cubic-like structure with a diameter of 2–3 μm, as shown in Fig.1a. Fig.1b-d show the FE-SEM images of CN/NN photocatalysts. With increasing dosage of urea, the surface of NN is covered with increasing dosage of CN. The loaded CN is also kept layered structure, as in Fig.1b-d. In Fig.1 (c) and (d) the surface of NN is full covered with layered CN.

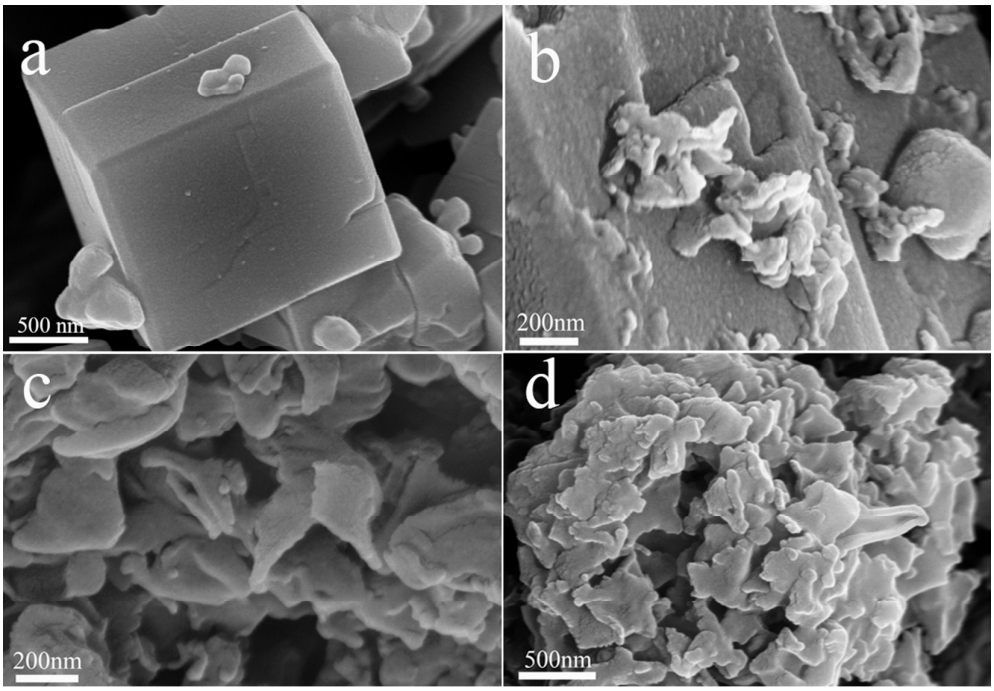

Fig.1. FE-SEM images of pure NN (a), 6-CN/NN (b), 8-CN/NN (c) and (d)

X-ray diffraction (XRD) analysis exhibits the lattice information, such as phase composition, purity and crystallinity. The XRD patterns for CN/NN composites with

different urea weights of 4g, 6g, 8g, 10g, and 12g are illustrated in Fig. 2. Pure NN is perovskite phase and CN is a class structure of graphene. With the increase of urea component in CN/NN composites, the intensity peak at 23.3° and 32.7°, which is identified as the main peak of the remnant NN phase, is gradually decreased, whereas, the intensity peak at 27.2° is increased. No other phases are found in CN/NN composites, suggesting that there is no appreciable chemical reaction between CN and NN. Well-crystallized NN powder synthesized with hydrothermal method possesses sharp diffraction peaks. In contrast, the peaks of CN are broader and less sharper, which may be owing to the smaller crystal size[38].

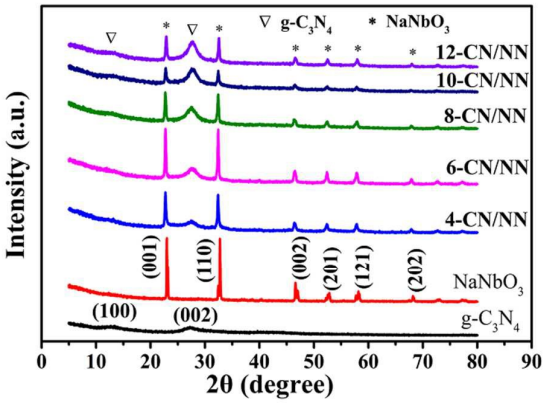

Fig. 2. XRD patterns of different photocatalysts

FT-IR spectra of CN/NN photocatalysts are shown in Fig. 3. The absorption peaks at 1251, 1326, 1416, 1570 and 1635 cm^{-1} are observed, which are due to the C-N and C=N stretching vibration modes, in FT-IR spectrum of pure CN. The peak at 812 cm^{-1} is associated with the characteristic breathing mode of s-triazine[39]. The spectrum of pure NN doesn't have obvious absorption peaks. It indicates that there is no H_2O and residual carbons in the materials[40], although, the pure NN is synthesized with hydrothermal method. It is obvious that the pure NN has a circular arc during 550 ~ 750cm^{-1}. The trend is also observed on 4-CN/NN, but is not observed on the other catalysts. It also indicates that when the adding dosage of urea is larger than the dosage of 6g, the surface of NN is completely covered by CN.

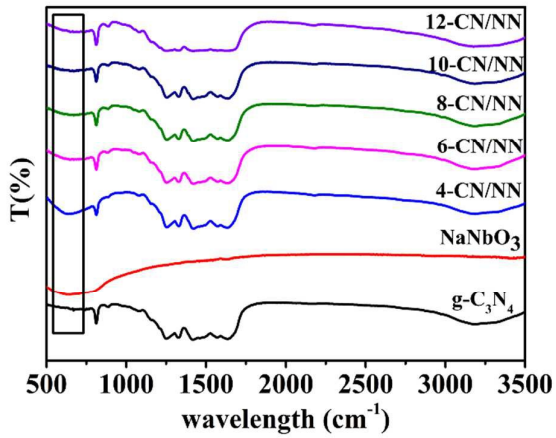

Fig. 3. FT-IR spectra of CN, NN and CN/NN hybrid materials

The chemical composition of the catalysts are analyzed by XPS, as shown in Fig. 4. Fig. 4a shows the XPS survey spectrum, which mainly exhibits the peaks of Na, Nb, O, C and N elements with sharp peaks appearing at bingding energies of 1073, 206, 532, 285 and 398eV, respectively. The adsorption peaks of Nb and Na are very low, and it may be owing to the coverage of NN by CN. Fig. 4b shows a high-resolution XPS spectrum of Nb3d. It is obvious that the binding energy of Nb3d is 206eV corresponding to its angular momentum of electrons[34]. Fig. 4c shows a high-resolution XPS spectrum of C1s of 8-CN/NN. The peak is related to coordination between carbon atoms and three nitrogen atoms in the CN lattice[41]. The N1s peak of CN is observed at 398.38eV in Fig. 4d, which originated from C-N=C coordination[42].

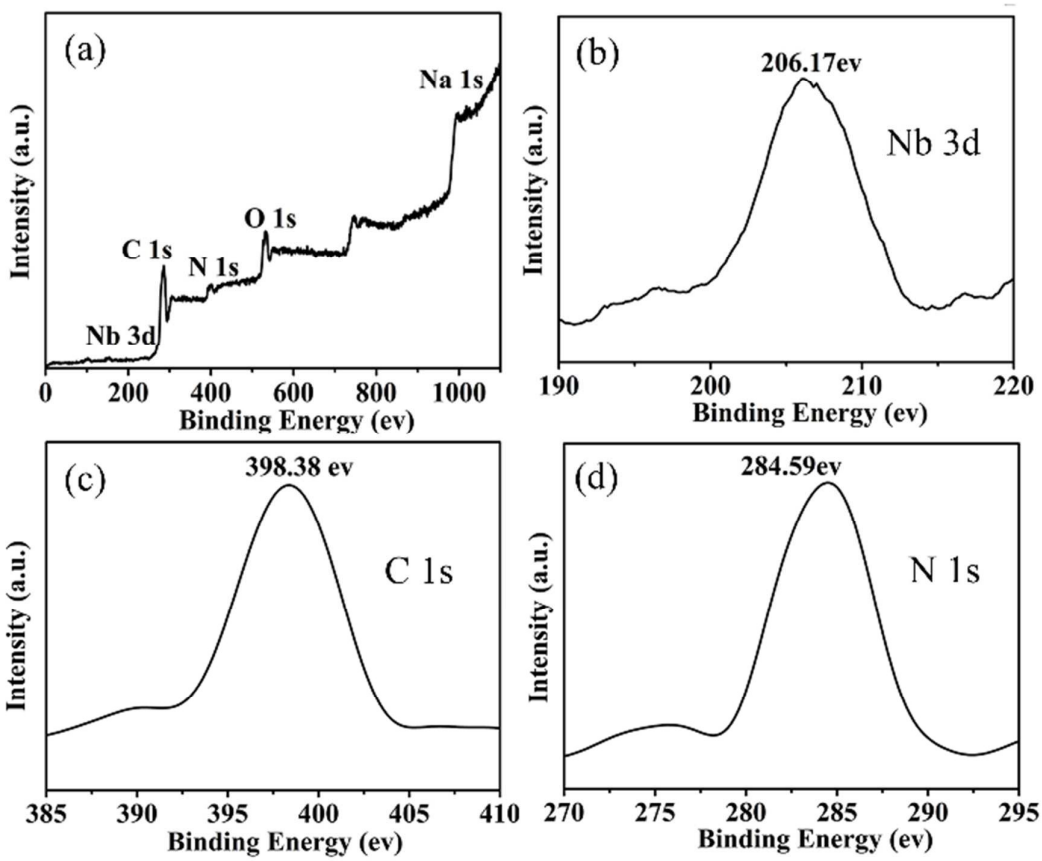

Fig. 4. XPS spectra of the 8-CN/NN sample: (a) the survey scan, (b) Nb 3d, (c) C 1s and (d) N 1s

A comparison of the optical properties of the CN/NN photocatalysts using UV–vis diffuse reflectance spectra analysis is shown in Fig. 5. Compared with the pure NN, the CN/NN samples show stronger absorbance in the wavelength range of 200 - 450 nm. The curve shape of UV-vis spectra of CN/NN are hardly changed with different dosage of urea, and they are also close to the curve shape of UV-vis spectra

of pure CN. The band gap energy of the prepared photocatalysts can be calculated by the following formula[43]:

$$\alpha h\nu = A(h\nu - Eg)^{n/2}$$

where α, h, v, A, and Eg are absorption coefficient, Planck constant, light frequency, proportionality and band gap energy, respectively; n keys the properties of the transition in a semiconductor (n = 1 for direct transition and n = 4 for indirect transition). The values of n for CN and NN are 4 and 1, respectively[44, 45]. By applying this equation, the band gap of NN and CN is 3.41 eV and 2.68 eV, respectively, which agrees with the previous reports[16, 32]. As is shown in Fig. 5 (a) and (b).

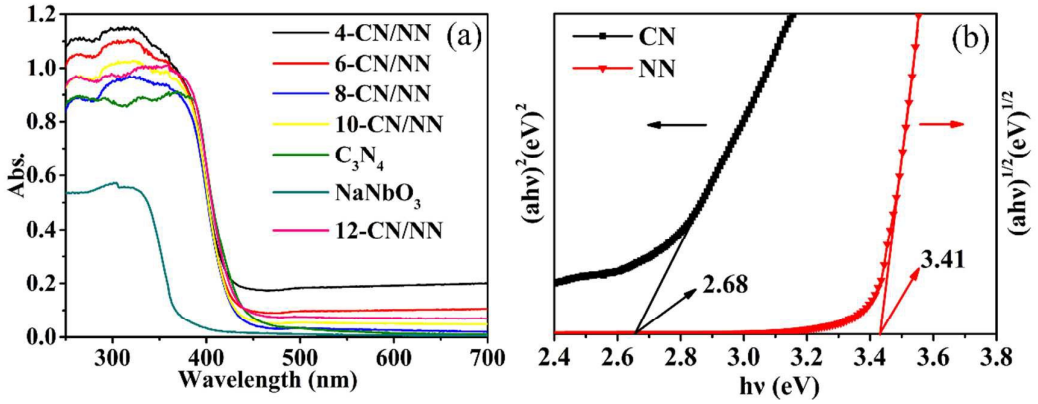

Fig. 5. UV–vis diffuse reflectance spectra of CN, NN and CN/NN composites.

3.2 Photocatalytic performances of the hybrid materials

Dyes are widely used in our lives that produce a lot of environmental problems. Treatment of dyes waste water is a challenge work for environmentalist. Photocataysis is a promising technology for dyes waste water purification. Thus, it is significant to investigate the photocatalytic activity of CN/NN under visible light.

Fig. 6 shows the RhB removal and degradation rates (*K*) under visible light irradiation with different photocatalysts. Pure NN is UV light driven photocatalyst, as its band gap energy is 3.41 eV. But RhB has a little degradation under visible light with pure NN. It may be due to the self-decomposition with visible light irradiation. The removal and degradation rates of pure NN are 12.6% and 0.0464h^{-1} respectively, and the removal and degradation rates are shown in Table 1. The removal and *K* of 8-CN/NN, 10-CN/NN and 12-CN/NN are larger than that of pure CN, and the removal and *K* of 4-CN/NN and 6-CN/NN are smaller than that of pure CN. The removal of 12-CN/NN is 95.6%, and it is largest in all these photocatalysts. The *K* of 8-CN/NN is 1.888h^{-1}, and it is largest in all these photocatalysts. It indicates that the weight ratio between CN and NN in 8-CN/NN is best for the separation of photoinduced holes and electrons. However, the photodegradation of RhB by each CN/NN photocatalysts all fit to pseudo first order kinetics well ($R^2 > 0.95$). In summary, the photocatalytic degradation of RhB by visible light driven photocatalyst—CN/NN indicates that CN/NN is a useful photocatalyst.

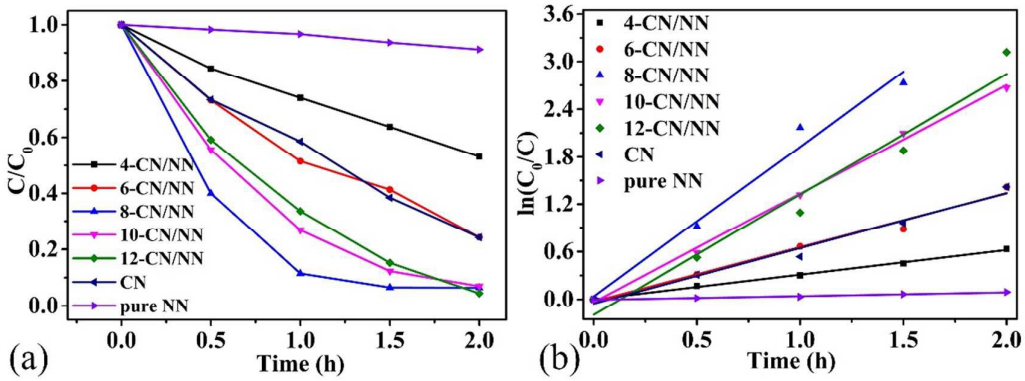

Fig. 6. Photocatalytic activities of as-prepared photocatalysts for RhB degradation under visible-light irradiation (a). Degradation kinetics of RhB after 2.0 h irradiation with visible-light (b). [RhB]=10mg/L, [photocatalyst]=0.5g/L.

Table 1. The photocatalytic activity parameters of different photocatalysts.

	4-CN/NN	6-CN/NN	8-CN/NN	10-CN/NN	12-CN/NN	CN	NN
Removal (%)	46.0	75.8	93.6	93.2	95.6	85.8	9.8
$K(h^{-1})$	0.309	0.681	1.888	1.369	1.519	0.697	0.046
R^2	0.997	0.977	0.972	0.996	0.953	0.976	0.974

Another two typical pollutants — MO and TC — are chosen as target contaminants to further evaluate photocatalytic activity of 8-CN/NN, as is shown in Fig. 7. The removal and *K* of MO and TC is investigated here. Similar to RhB degradation, the photocatalyst shows high photocatalytic activity for MO and TC removal. After 3h irradiation of visible light, 77.2% of MO degradation and 73.3% of TC degradation are achieved, as is shown in Table 2. The removal and *K* of MO and TC are smaller than that of RhB. The *K* of MO and TC are 0.494 and 0.385, respectively. They are all smaller than that of RhB. The degradation of RhB, MO and TC fit the pseudo first order kinetics models ($R^2 \geq 0.94$) well.

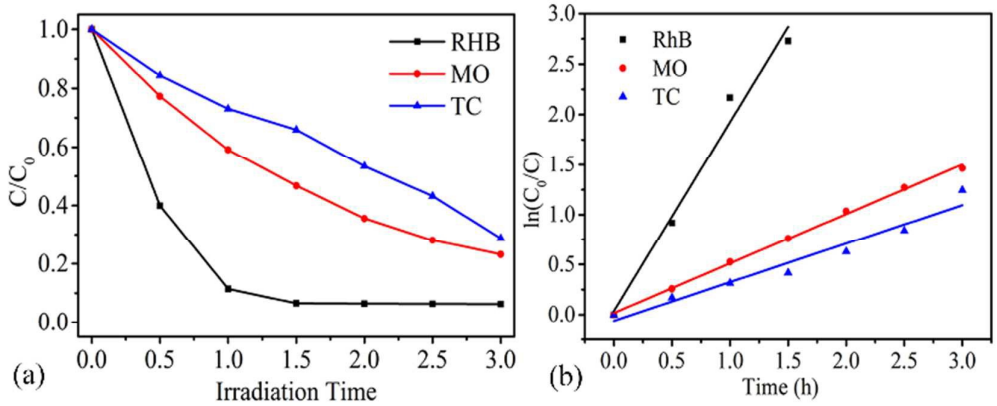

Fig. 7. Photocatalytic degradation rates for RhB, MO and TC by 8-CN/NN under visible-light irradiation (a). Degradation kinetics of RhB, MO and TC after 2.0 h irradiation with visible-light (b). [RhB]=10mg/L, [photocatalyst]=0.5g/L.

Table 2. The photocatalytic activity parameters of RhB, MO and TC degradation by 8-CN/NN.

	RhB	MO	TC
Removal (%)	93.6	77.2	73.3
K (h^{-1})	1.888	0.494	0.385
R^2	0.972	0.998	0.946

The stability of photocatalyst is of paramount importance for practical application, since it can promote significantly reducing the operational cost of photocatalytic process, thus making the application of photocatalysis in dye wastewater treatment to be foreseeable. After five recycling runs, there is no obvious change in the photocatalytic degradation efficiencies of RhB by 8-CN/NN, as is shown in Fig. 8(a). The stability of photocatalyst is monitored by XRD, as is shown in Fig. 8(b). After 5 cycles, the phase of the NN and CN is intact, implying that the heterostructure of the photocatalyst maintains stability even after 5 cycles photocatalysis reactions.

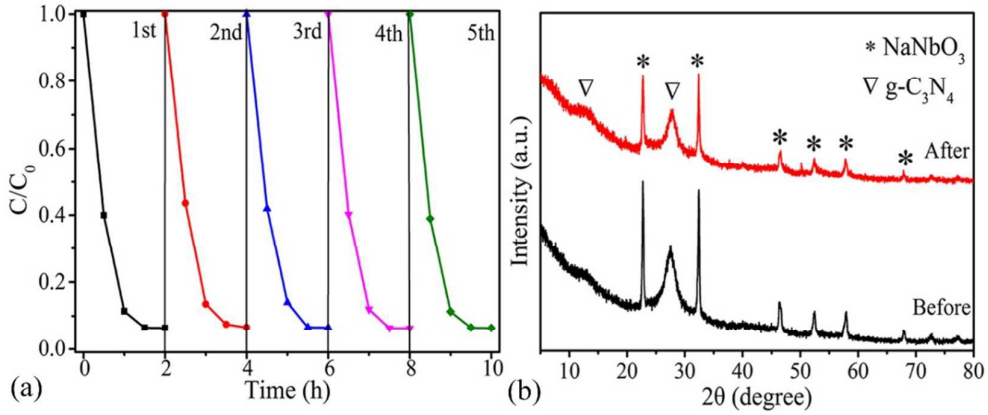

Fig. 8. Degradation efficiency of 8-CN/NN heterostructure with increasing number of catalytic cycles (a), XRD patterns of 8-CN/NN heterostructure before and after photocatalytic reaction.

3.3 Mechanism of enhanced photocatalytic activity

The enhancement of photodegradation efficiency for CN/NN composites compared to pure CN photocatalyst can be ascribed to the appropriate band structure. The band-edge potentials of CB and VB, designated as E_{CB} and E_{VB}, can be calculated from the following equation:

$$E_{VB} = \chi - E_0 + \frac{1}{2}E_g$$

$$E_{CB} = \chi - E_0 - \frac{1}{2}E_g$$

in which χ is the absolute electronegativity of the semiconductor, determined by the geometric mean of the absolute electronegativity of constituent atoms, which is defined as the arithmetic mean of the atomic electron affinity and the first ionization

energy; E_0 is the energy of free electrons on the hydrogen scale; and Eg is the band gap of the semiconductor[46, 47]. E_{CB} and E_{VB} of NN are determined to be -0.60 and 2.81 eV, while those of CN are -1.08 and 1.60 eV. On the basis of the alignment of their energy levels, as is shown in Fig. 9, an illustration of possible electron transfer behavior is proposed. Under the irradiation of visible light, the photoinduced-electrons are excited from the valence band (VB) of CN in NN/CN heterostructures to its conduction band (CB), thereby producing the active species — electron and hole. Simultaneously, the photoinduced electrons can fast transfer to the CB of NN, which can be further trapped by molecular oxygen on the surface of NN, to activate molecular oxygen to superoxide radical anion and other radicals. These processes efficiently lower the recombination rates of electron−hole pairs and prolonging the charge carriers' lifetime. The photogenerated hole on the VB of CN can transfer to surface of CN and be trapped by the OH^-, forming the OH•, which is also an active specie in the photodegradation reactions.

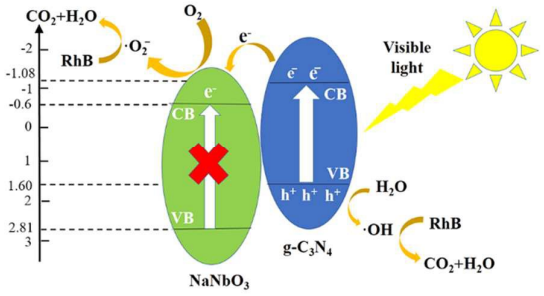

Fig. 9. Schematic diagram of electron-hole pairs' separation between p-type CN and n-type NN.

For the better application of NN/CN photocatalyst in pollutants photocatalytic degradation, it is imperative to understand the mechanism of photocatalysis of RhB under visible light irradiation. To explore the mechanism of photocatalytic degradation of RhB by NN/CN heterostructure photocatalysts, ESR spectrum and radical scavenger experiments are employed to ascertain the active species. ESR spectrums are used for the detection of the production of OH• and $O_2^{\bullet-}$. Benzoquinone (BQ) as a scavenger for $O_2^{\bullet-}$, EDTA for h^+ and tertiary butanol (TBA) for OH• are employed to observe the direct influence on the degradation rates of each radicals. The addition of quenchers to the RhB solution are all prior to the addition of photocatalysts. As a consequence of capture, photocatalytic degradation of RhB will be influenced and photocatalytic efficiency is changed. The effects of a series of scavengers on the photodegradation efficiency are shown in Fig. 10. As is shown in Fig. 10(a), the degradation efficiency of RhB decreases rapidly from 93.61% to 34.03% after the addition of BQ, indicating that $O_2^{\bullet-}$ is the main active species in the photodegradation process. While TBA is added, the photodegradation efficiency of

RhB decrease from 93.61% to 84.93%. It is indicated that OH• promotes the photocatalytic efficiency, but is not the main active species. However, while the EDTA is adding, the degradation efficiency increases a little from 93.61% to 94.60%. It may be due to the quenching of h^+, which promotes the separation of photoinduced holes and electrons. Then the degradation efficiency is improved. The ESR spectra also reveals the proof of these phenomenons, as is shown in Fig. 10(b). In these ESR detection, 10 mg samples and 50 μL DMPO are dissolved in 0.5 mL deionized water and stirred for 10 min, which is used in the detection of hydroxyl radicals (DMPO–OH•). 10 mg samples and 50 μL DMPO are dissolved in 0.5 mL CH_3OH and stirred for 10 min, which is used in the detection of superoxide radicals (DMPO– $O_2^{\bullet-}$). Before the irradiation, there are no characteristic peak of OH• and $O_2^{\bullet-}$. After the irradiation (60s), the characteristic peak intensity of $O_2\bullet^-$ is much larger than that of OH•. It is also accord with the consequence of radical scavenger experiments, that the $O_2^{\bullet-}$ is the main active species and the OH• promotes the photocatalytic efficiency, but is not the main active species.

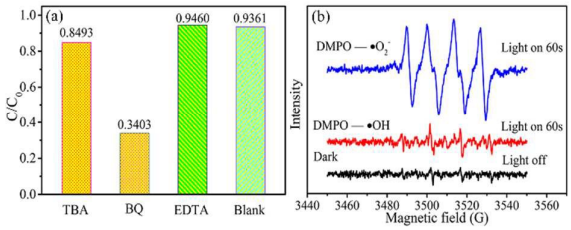

Fig. 10. (a) Effects of a series of scavengers on the degradation efficiency of RhB by 8-CN/NN sample (the dosage of scavengers = 5 mmol/L, illumination time t = 2h). (b) ESR signals of the DMPO– $O_2^{\bullet-}$ and DMPO– OH•.

On the basis of the above consequence, we propose a plausible mechanism for the photodegradation of RhB over NN/CN heterostructures.

$$C_3N_4+hv\rightarrow C_3N_4(e^-_{CB}+h^+_{VB})$$
$$C_3N_4(e^-_{CB})+NaNbO_3\rightarrow C_3N_4+NaNbO_3(e^-_{CB})$$
$$NaNbO_3(e^-_{CB})+O_2\rightarrow NaNbO_3+O_2^{\bullet-}$$
$$O_2^{\bullet-}+RhB\rightarrow\cdots\rightarrow CO_2+H_2O$$
$$C_3N_4(h^+_{VB})+OH^-\rightarrow C_3N_4+\bullet OH$$
$$\bullet OH+RhB\rightarrow\cdots\rightarrow CO_2+H_2O$$

where e^-_{CB} and h^+_{VB} stand for the electron in the conduction band and hole in the valence band, respectively.

In summary, the NN/CN photocatalysts owns efficiency and stability in photodegradation process. With the suited CB and VB of two pure phase photocatalysts, the main active specie is $O_2\bullet^-$ and the OH• also plays a role in the photodegradation process. The exploration of active species of photocatalyst will promote the further application of photocatalysis in wastewater treatment.

4. Conclusions

In this work, an enhanced visible-light-driven photocatalyst of $NaNbO_3$/g-C_3N_4 by the combination of $NaNbO_3$ and g-C_3N_4 is designed. Among hybrid photocatalysts, the 8-CN/NN sample exhibited optimal photocatalytic activity for RhB degradation under visible-light irradiation. Furthermore, the photocatalyst could also efficiently remove other organic pollutants such as MO and TC in wastewater. And the photodegradation of RhB, MO and TC all fit to pseudo first order kinetics by all CN/NN photocatalysts. In addition, the cycling experiments reveals that the photocatalyst possesses great stability. In general, the CN sensitized and substrated by NN can address the problem of low photocatalytic activity of CN alone. This work may provide a promising approach for treatment of wastewater.

Acknowledgement:
The authors would like to acknowledge the National Natural Science Foundation of China (21276116, 21477050, 21301076, 21303074 and 21201085), the Chinese-German Cooperation Research Project (GZ1091), the Excellent Youth Foundation of Jiangsu Scientific Committee (BK20140011), the Open Project of State Key Laboratory of Rare Earth Resource Utilizations (RERU2014010), the Program for New Century Excellent Talents in University (NCET-13-0835), the Henry Fok Education Foundation (141068) and Six Talents Peak Project in Jiangsu Province (XCL-025), International Scientific and Technological Cooperation in Changzhou (CZ20140017).

References

1. Akira Fujishima, K. Honda, Nature 1972, 238, 37 - 38.
2. R. Asahi, T. Morikawa, T. Ohwaki, K. Aoki and Y. Taga, *Science*, 2001, 293, 269-271.
3. G. Liu, Y. Zhao, C. Sun, F. Li, G. Q. Lu and H.-M. Cheng, *Angewandte Chemie-International Edition*, 2008, 47, 4516-4520.
4. H. G. Yang, C. H. Sun, S. Z. Qiao, J. Zou, G. Liu, S. C. Smith, H. M. Cheng and G. Q. Lu, *Nature*, 2008, 453, 638-U634.
5. W. Zhang, B. S. Naidu, J. Z. Ou, A. P. O'Mullane, A. F. Chrimes, B. J. Carey, Y. Wang, S.-Y. Tang, V. Sivan, A. Mitchell, S. K. Bhargava and K. Kalantar-zadeh, *Acs Applied Materials & Interfaces*, 2015, 7, 1943-1948.
6. S. Yu, T. Zhang, Y. Xie, Q. Wang, X. Gao, R. Zhang, L. Zhang and H. Su, *International Journal of Hydrogen Energy*, 2015, 40, 870-877.
7. S. D. Verberne-Sutton, R. D. Quarels, X. Zhai, J. C. Garno and J. R. Ragains, *Journal of the American Chemical Society*, 2014, 136, 14438-14444.
8. R. Konta, T. Ishii, H. Kato and A. Kudo, *Journal of Physical Chemistry B*, 2004, 108, 8992-8995.
9. Q. Wang, S. Yu, Z. Tan, R. Zhang, Z. Li, X. Gao, B. Shen and H. Su, *Crystengcomm*, 2015, 17, 671-677.
10. K. Maeda, K. Teramura and K. Domen, *Catalysis Surveys from Asia*, 2007, 11, 145-157.

11. K. Maeda, T. Takata, M. Hara, N. Saito, Y. Inoue, H. Kobayashi and K. Domen, *Journal of the American Chemical Society*, 2005, 127, 8286-8287.
12. P. V. Kamat, *Journal of Physical Chemistry C*, 2007, 111, 2834-2860.
13. Y. Zheng, J. Liu, J. Liang, M. Jaroniec and S. Z. Qiao, *Energy & Environmental Science*, 2012, 5, 6717-6731.
14. D. J. Martin, K. Qiu, S. A. Shevlin, A. D. Handoko, X. Chen, Z. Guo and J. Tang, *Angewandte Chemie-International Edition*, 2014, 53, 9240-9245.
15. A. Du, S. Sanvito, Z. Li, D. Wang, Y. Jiao, T. Liao, Q. Sun, Y. H. Ng, Z. Zhu, R. Amal and S. C. Smith, *Journal of the American Chemical Society*, 2012, 134, 4393-4397.
16. F. Su, S. C. Mathew, G. Lipner, X. Fu, M. Antonietti, S. Blechert and X. Wang, *Journal of the American Chemical Society*, 2010, 132, 16299-16301.
17. J. Ran, J. Zhang, J. Yu, M. Jaroniec and S. Z. Qiao, *Chemical Society Reviews*, 2014, 43, 7787-7812.
18. J. Zhu, P. Xiao, H. Li and S. A. C. Carabineiro, *Acs Applied Materials & Interfaces*, 2014, 6, 16449-16465.
19. J. W. Liu, G. Chen, Z. H. Li and Z. G. Zhang, *International Journal of Hydrogen Energy*, 2007, 32, 2269-2272.
20. H. Shi, G. Chen, C. Zhang and Z. Zou, *Acs Catalysis*, 2014, 4, 3637-3643.
21. X. Wang, S. Blechert and M. Antonietti, *Acs Catalysis*, 2012, 2, 1596-1606.
22. Y. Wang, X. Wang and M. Antonietti, *Angewandte Chemie-International Edition*, 2012, 51, 68-89.
23. H. Li, J. Liu, W. Hou, N. Du, R. Zhang and X. Tao, *Applied Catalysis B-Environmental*, 2014, 160, 89-97.
24. S. Kumar, T. Surendar, A. Baruah and V. Shanker, *Journal of Materials Chemistry A*, 2013, 1, 5333-5340.
25. J. L. Gunjakar, I. Y. Kim, J. M. Lee, N.-S. Lee and S.-J. Hwang, *Energy & Environmental Science*, 2013, 6, 1008-1017.
26. Y. Zhang, T. Mori, J. Ye and M. Antonietti, *Journal of the American Chemical Society*, 2010, 132, 6294-+.
27. M. Zhang, J. Xu, R. Zong and Y. Zhu, *Applied Catalysis B-Environmental*, 2014, 147, 229-235.
28. Y. Hou, Z. Wen, S. Cui, X. Guo and J. Chen, *Advanced Materials*, 2013, 25, 6291-6297.
29. L. Sun, X. Zhao, C.-J. Jia, Y. Zhou, X. Cheng, P. Li, L. Liu and W. Fan, *Journal of Materials Chemistry*, 2012, 22, 23428-23438.
30. K. Wu, Q. Li, Y. Jia, J. R. McBride, Z.-x. Xie and T. Lian, *ACS Nano*, 2015, 9, 961-968.
31. S. Chen, L. Ji, W. Tang and X. Fu, *Dalton Transactions*, 2013, 42, 10759-10768.
32. J. H. Jung, M. Lee, J.-I. Hong, Y. Ding, C.-Y. Chen, L.-J. Chou and Z. L. Wang, *ACS Nano*, 2011, 5, 10041-10046.
33. K. E. Johnston, C. C. Tang, J. E. Parker, K. S. Knight, P. Lightfoot and S. E. Ashbrook, *Journal of the American Chemical Society*, 2010, 132, 8732-8746.
34. H. Xua, C. Liu, H. Li, Y. Xu, J. Xia, S. Yin, L. Liu and X. Wu, *Journal of Alloys and Compounds*, 2011, 509, 9157-9163.
35. J. Lv, T. Kako, Z. Li, Z. Zou and J. Ye, *Journal of Physical Chemistry C*, 2010, 114, 6157-6162.

36. C. Yan, L. Nikolova, A. Dadvand, C. Harnagea, A. Sarkissian, D. F. Perepichka, D. Xue and F. Rosei, *Advanced Materials*, 2010, 22, 1741-+.
37. G. Li, N. Yang, W. Wang and W. F. Zhang, *Journal of Physical Chemistry C*, 2009, 113, 14829-14833.
38. N. Zhang, J. Shi, S. S. Mao and L. Guo, *Chemical Communications*, 2014, 50, 2002-2004.
39. Y. Wang, R. Shi, J. Lin and Y. Zhu, *Energy & Environmental Science*, 2011, 4, 2922-2929.
40. W. Liu, H. Wang and K. Li, *Journal of Sol-Gel Science and Technology*, 2010, 55, 229-234.
41. A. Thomas, A. Fischer, F. Goettmann, M. Antonietti, J.-O. Mueller, R. Schloegl and J. M. Carlsson, *Journal of Materials Chemistry*, 2008, 18, 4893-4908.
42. H. Shi, Z. Li, J. Kou, J. Ye and Z. Zou, *Journal of Physical Chemistry C*, 2011, 115, 145-151.
43. A. Kudo and Y. Miseki, *Chemical Society Reviews*, 2009, 38, 253-278.
44. S. Chen, Y. Hu, L. Ji, X. Jiang and X. Fu, *Applied Surface Science*, 2014, 292, 357-366.
45. S. Chen, Y. Hu, S. Meng and X. Fu, *Applied Catalysis B-Environmental*, 2014, 150, 564-573.
46. X. Guan and L. Guo, *Acs Catalysis*, 2014, 4, 3020-3026.
47. C. Li, P. Zhang, R. Lv, J. Lu, T. Wang, S. Wang, H. Wang and J. Gong, *Small*, 2013, 9, 3951-3956.

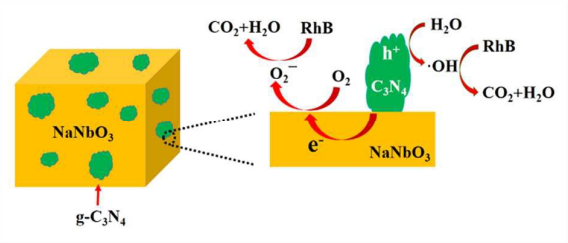

g-C_3N_4-sensitized and $NaNbO_3$-substrated II-type heterojunction with enhanced photocatalytic activity